Renewable Energy 76 (2015) 662–669

Contents lists available at ScienceDirect

Renewable Energy

journal homepage: www.elsevier.com/locate/renene

Digital proportional multi-resonant current controller for improving grid-connected photovoltaic systems

Pedro M. Almeida [a, *], Pedro G. Barbosa [a], Janaina G. Oliveira [a], Jorge L. Duarte [b], Paulo F. Ribeiro [c]

[a] Power Electronics and Automation Group, Electrical Engineering Program, Federal University of Juiz de Fora, Juiz de Fora, MG, 36.036-900, Brazil
[b] Department of Electrical Engineering, Eindhoven University of Technology, Eindhoven, 5600, MB, The Netherlands
[c] Electrical Engineering Institute, Federal University of Itajubá, Itajubá, MG, 37.500-903, Brazil

ARTICLE INFO

Article history:
Received 1 March 2014
Accepted 27 November 2014
Available online 12 December 2014

Keywords:
Digital controller
Resonant compensator
Current controller
Grid-connected
Photovoltaic
Discrete-time modeling

ABSTRACT

This paper presents the modelling and design steps of a digital proportional multi-resonant controller used in a grid-connected photovoltaic (PV) system. It is shown that the use of only one Proportional-Resonant (PR) compensator, tuned to the system fundamental frequency, may have its effectiveness compromised due to nonlinearities in the system components. To overcome this drawback and improve the system's output current waveform, a multi-resonant controller is introduced. The performance of the discrete-time designed controller is tested on a grid-connected photovoltaic power plant. Experimental results obtained with the operation of a 30 kWp PV system connected to a distribution network, using only the leakage inductances of a connection transformer as passive filter are presented and discussed to demonstrate the performance of the designed control strategy.

1. Introduction

The integration of small and medium capacity sustainable sources-based distributed generation systems into the electric grid is a fast and environmentally friendly way to meet growing electricity demand in developed and developing countries. Among renewable energy sources, photovoltaic (PV) systems are one of the most promising, with a robust and exponential growth [1].

Several converter topologies have been proposed to implement the inverter and interface it with the grid [2]. They can be classified as single-phase or three-phase, with one or more stages. Another categorization divide the topologies into three major classes: (*i*) Low-frequency transformer coupling; (*ii*) High-frequency transformer; and (*iii*) Transformerless topologies.

Transformerless topologies have the advantage of higher efficiency and reduced size. However, they have issues with respect to ground leakage current and DC current injection into the grid. On the other hand, when galvanic isolation is mandatory, topologies based on transformers must be used. Although high frequency transformers eliminate the ground leakage currents, they do not prevent DC current injection [3].

Based on the fact that the IEC 61727 [4] and IEEE 1547 [5] standards set limits for the maximum allowable amount of DC current which can be injected into the grid, the classical solution with line frequency transformer between the converter and the grid will be used in this work. This solution in addition to preventing the DC current injection, guarantees galvanic isolation and voltage level adjustment.

Fig. 1 shows a PV system single line diagram. It consists of PV arrays connected to a voltage source converter (VSC) input terminals, along with acquisition system, signal conditioning, and controls. The interface between the VSC and the grid is done only by a coupling transformer, where its leakage inductances are used to attenuate the switching frequency current harmonics. This approach eliminates the output low-pass filter hence reducing the system size and cost.

Several strategies are used to control the interface converter. Historically, the first control methods were developed in the

* Corresponding author.
E-mail address: pedro.machado@engenharia.ufjf.br (P.M. Almeida).

http://dx.doi.org/10.1016/j.renene.2014.11.087
0960-1481/

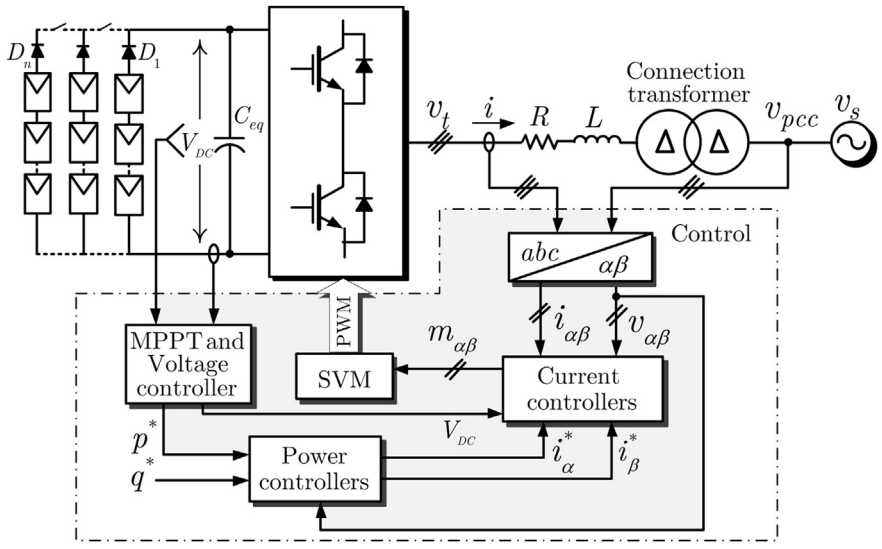

Fig. 1. Schematic diagram of a grid-tied PV system.

natural or *abc* reference frame [6]. They use nonlinear controllers (*e.g.* hysteresis controllers) and have the disadvantage of requiring high sampling frequencies and to switch the converter semiconductors with a variable frequency.

As an alternative, the synchronous reference frame can be used. In the *dq*0 frame, the variables are referred to a coordinate system synchronized with the grid AC signals [7]. The advantage of this strategy is that the signals in the synchronous frame are no longer AC, but DC signals. This allows the design of simpler linear controllers (*e.g.* proportional-integral (PI)) [8]. Nevertheless, a *Phase Locked-Loop* (PLL) is required to estimate the angle of the grid voltages in order to guarantee the correct transformation [9,10].

Another approach is the use of the stationary $\alpha\beta 0$ reference frame. This strategy, when applied to a three phase, three-wire system reduces the number of controllable variables [6,11]. However, as with the natural reference frame, the currents and voltages are time varying waveforms.

This paper describes the design of a digital proportional multi-resonant current controller. The objective is to compensate distorted currents generated by a photovoltaic system, especially when the PV system is connected to the grid without output passive filters.

Initially an analytical model is presented in the *abc* frame and then it is discretized and transformed to an $\alpha\beta 0$ frame. The aforementioned model is used to design the inner current compensators. When the system is connected to the grid, with only a Proportional-resonant (PR) controller tuned to the fundamental frequency, distorted currents are generated due to the nonlinear behaviour of the connection transformer. With the design and the inclusion of additional resonant controllers, the distorted current is compensated. Experimental results are presented to demonstrate and validate the performance of the digital proportional multi-resonant controller.

2. AC-side model

Based on Fig. 1, and neglecting the high frequency switching harmonics, the following system can be written for the converter's AC side

$$\frac{d}{dt}\begin{bmatrix} i_a(t) \\ i_b(t) \\ i_c(t) \end{bmatrix} = \begin{bmatrix} -\frac{R}{L} & 0 & 0 \\ 0 & -\frac{R}{L} & 0 \\ 0 & 0 & -\frac{R}{L} \end{bmatrix} \begin{bmatrix} i_a(t) \\ i_b(t) \\ i_c(t) \end{bmatrix} + \begin{bmatrix} \frac{1}{L} & 0 & 0 \\ 0 & \frac{1}{L} & 0 \\ 0 & 0 & \frac{1}{L} \end{bmatrix} \begin{bmatrix} v_a(t) \\ v_b(t) \\ v_c(t) \end{bmatrix}, \tag{1}$$

where $i_a(t)$, $i_b(t)$, and $i_c(t)$ are the instantaneous currents at the converter's terminals; $v_a(t) = (v_{t,a}(t) - v_{a,pcc}(t)/N)$, $v_b(t) = (v_{t,b}(t) - v_{b,pcc}(t)/N)$, and $v_c(t) = (v_{t,c}(t) - v_{c,pcc}(t)/N)$; $v_{t,a}(t), v_{t,c}(t)$, and $v_{t,c}(t)$ are the instantaneous voltages at the converter's AC terminals; $v_{a,pcc}(t), v_{b,pcc}(t)$, and $v_{c,pcc}(t)$ are the instantaneous voltages at the point of common coupling (PCC); N is the transformer turns ratio; L and R are the equivalent leakage inductance and the series resistance of the connection transformer windings reflected to the primary side, respectively.

Applying the zero-order hold method, as explained in Appendix A [12], to discretize (1), yields.

The discretization of (1) by using the *zero-order hold* (ZOH) method (Appendix A) yields,

$$\begin{bmatrix} i_a(n+1) \\ i_b(n+1) \\ i_c(n+1) \end{bmatrix} = \mathbf{\Phi} \begin{bmatrix} i_a(n) \\ i_b(n) \\ i_c(n) \end{bmatrix} + \mathbf{\Gamma} \begin{bmatrix} v_a(t) \\ v_b(t) \\ v_c(t) \end{bmatrix}, \tag{2}$$

where $(n+1)$ and (n) represents the discrete time $t_{n+1} = (n+1)T_s$ and $t_n = nT_s$, respectively; n is a positive integer that represents the sampling time and T_s is the sampling time. The matrices $\mathbf{\Phi}$ and $\mathbf{\Gamma}$ are calculated by

$$\mathbf{\Phi} = \begin{bmatrix} e^{-\left(\frac{RT_s}{L}\right)} & 0 & 0 \\ 0 & e^{-\left(\frac{RT_s}{L}\right)} & 0 \\ 0 & 0 & e^{-\left(\frac{RT_s}{L}\right)} \end{bmatrix}, \tag{3}$$